



Fuel Composition and Diluent Effect on Gas Transport and Performance of Anode-Supported SOFCs

Yi Jiang* and Anil V. Virkar*^z

Department of Materials Science and Engineering, University of Utah, Salt Lake City, Utah 84112, USA

Anode-supported solid oxide fuel cells (SOFCs) with Ni+yttria-stabilized zirconia (YSZ) anode, YSZ-samarium-doped ceria (SDC) bilayer electrolyte, and Sr-doped LaCoO₃ (LSC)+SDC cathode were fabricated. Fuel used consisted of H₂ diluted with He, N₂, H₂O, or CO₂, mixtures of H₂ and CO, and mixtures of CO and CO₂. Cell performance was measured at 800°C with the above-mentioned fuel gas mixtures and air as oxidant. For a given concentration of the diluent, cell performance was higher with He as the diluent than with N₂ as the diluent. Mass transport through porous Ni-YSZ anode for H₂-H₂O, CO-CO₂ binary systems, and H₂-H₂O-diluent gas ternary systems was analyzed using multicomponent gas diffusion theory. At high concentrations of diluent, the maximum achievable current density was limited by the anodic concentration polarization. From this measured limiting current density, the corresponding effective gas diffusivity was estimated. Highest effective diffusivity was estimated for fuel gas mixtures containing H₂-H₂O-He mixtures (~0.55 cm²/s), and the lowest for CO-CO₂ mixtures (~0.07 cm²/s). The lowest performance was observed with CO-CO₂ mixture as a fuel, which in part was attributed to the lowest effective diffusivity of the fuels tested and higher activation polarization.

© 2003 The Electrochemical Society. [DOI: 10.1149/1.1579480] All rights reserved.

Manuscript submitted April 21, 2002; revised manuscript received January 20, 2003. Available electronically May 30, 2003.

Recent work has demonstrated that anode-supported solid oxide fuel cells (SOFCs) exhibit high performance at intermediate temperatures. Maximum power densities as high as 1.8-1.9 W/cm² have been reported at 800°C for anode-supported single cells.¹⁻⁴ In a typical anode-supported SOFC, the anode support is a Ni-yttria-stabilized zirconia (YSZ) cermet between ~0.5 and 2 mm thick. The electrolyte is a thin (~10 μm), dense YSZ film supported on a porous anode substrate. The cathode is usually a porous mixture of strontium-doped manganite, La_{1-x}Sr_xMnO_{3-δ} (LSM), and YSZ,¹⁻³ or a porous mixture of strontium-doped cobaltite, La_{1-x}Sr_xCoO_{3-δ} (LSC), and Sm-doped CeO₂ (SDC).⁴ In addition, single-phase, mixed ionic-electronic conductors (MIEC) materials have also been used in high-performance fuel cells. The use of thin electrolyte film results in a relatively low ohmic contribution to the total cell resistance, which makes it possible to operate anode-supported SOFCs at 800°C or lower and thereby realize the benefits of a lower temperature operation, such as the use of inexpensive metallic interconnect. One of the potential benefits of SOFCs over low-temperature fuel cells, such as proton exchange membranes (PEMs) is fuel flexibility, because SOFCs can potentially operate on various fuels including hydrogen, carbon monoxide, methane, and other hydrocarbon fuels without the problem of CO poisoning. Recent work has also shown that it may be possible to operate SOFCs directly on a number of hydrocarbon fuels, without the necessity of reforming.⁵⁻⁸ However, in anode-supported SOFCs, significant losses may occur due to the resistance to the transport of fuel gas through a relatively thick anode, and especially at high fuel utilizations. The losses at the anode are expected to become even more severe when the fuel used contains gaseous species of molecular weights much greater than that of hydrogen (H₂), such as CO, CH₄, or other hydrocarbons. It is thus imperative that a thorough investigation of the transport characteristics of various gaseous species through porous anodes be conducted to fully assess anodic concentration polarization losses in anode-supported SOFCs. Gas transport through porous bodies, and the effects of parameters such as volume fraction porosity, morphology of pores, and pore size, have been studied in great detail.^{9,10} However, there is limited information available in the literature pertaining to SOFCs.

Insofar as SOFCs are concerned, there are only a couple of papers in the literature examining gas-transport phenomena in porous anodes with emphasis on hydrocarbon fuels. Lehnert *et al.*¹¹ conducted a simulation study of gas transport coupled with steam-

reforming and gas shift reactions in a Ni-YSZ porous anode using a single-channel model. The study showed that the anode structural parameter, defined as the ratio of porosity, V_v , to tortuosity, τ , had a significant effect on methane conversion rate. A reduction of the structural parameter by 26% lowered the methane conversion by 12%. No electrochemical overpotential or performance measurements, however, were correlated with gas transport in this study. Yakabe *et al.*¹² studied gas transport in H₂-H₂O and CO-CO₂ binary systems through porous anodes. Under a constant current density, the concentration distributions of reactants H₂ and CO along the direction normal and parallel to the electrode/electrolyte interface were evaluated. The results showed that the calculated concentration polarization was much higher for CO-CO₂ than for H₂-H₂O due to the much lower diffusivity of CO-CO₂. These computational results were also compared with experimental measurements. The results on steam-reformed methane as fuel indicated that the gas shift reaction in porous anodes effectively reduces concentration polarization.

In the present paper, we address mass transport in porous anode support of an SOFC. Studies were conducted on a variety of fuel mixtures, such as as-received H₂; mixtures of H₂ with inert gases such as He, and N₂; H₂-H₂O, H₂-CO, and H₂-CO₂ mixtures; and CO-CO₂ mixtures. All tests were conducted on one cell to ensure that possible differences due to cell-to-cell variations are eliminated. Mass transport in these binary and ternary systems was analyzed. This included the estimation of effective diffusivities of gaseous species through porous anodes, the effect of diluents on transport, and the associated concentration polarization. In the case of mixtures of CO and H₂, the effect of *in situ* gas shift reaction was examined.

Experimental

Cell fabrication.—While only measurements on one cell are reported, a number of cells were fabricated. Single cells consisted of a Ni+YSZ anode substrate, a Ni+YSZ anode interlayer, a YSZ-SDC bilayer thin-film electrolyte, a LSC+SDC cathode interlayer, and a LSC cathode current collector layer. The procedure for preparing an anode substrate and an anode interlayer was described elsewhere in detail¹³ and is briefly described here. NiO and YSZ powders from commercial sources were mixed in requisite proportions and ball-milled in alcohol, dried, and screened through a 150 mesh sieve. A circular disk ~1.2 mm thick and ~3 cm diam was uniaxially die-pressed and presintered at 1000°C for 1 h. The disk was then coated with a slurry of NiO+YSZ anode interlayer and fired again at the same temperature for 1 h to form a NiO+YSZ interlayer ~20 μm thick. YSZ and SDC layers were applied on the anode interlayer

* Electrochemical Society Active Member.

^z E-mail: anil.virkar@m.cc.utah.edu

surface sequentially using YSZ and SDC suspensions made from YSZ and 20 mol% samarium-doped CeO₂ powders, dispersed ultrasonically in appropriate amounts of suitable liquids. Then the bilayer electrolyte-anode substrate assembly was sintered in air at a temperature between 1400 and 1500°C to form a dense, well-bonded YSZ-SDC bilayer electrolyte-anode structure. The thickness of the SDC layer was around 3 μm and the total thickness of the YSZ-SDC bilayer electrolyte thin film was ~10 μm. The thin SDC layer, as part of the electrolyte, served as a barrier, which prevented a direct contact between YSZ and LSC. In this manner, the possible chemical reaction between YSZ and LSC, which can form insulating La₂Zr₂O₇ during a high-temperature firing step, could be prevented.

The porous cathode interlayer was a composite of 50 wt % strontium-doped lanthanum cobaltite [La_{1-x}Sr_xCoO_{3-δ} (LSC), $x = 0.3-0.7$] and 50 wt % SDC. The cathode interlayer was applied by screen-printing, followed by firing at a temperature between 1050 and 1300°C for 2 h to form a good bond between the SDC layer and the cathode interlayer. The thickness of the interlayer after firing was ~20 μm. On top of the interlayer, a porous layer of LSC was applied, followed by firing at a temperature between 1050 and 1300°C for 1 h in air. The final anode thickness and the disk diameter were 1.1 and 27.7 mm, respectively. The cathode area was 1.1 cm².

The measurement of cell performance.—The cell was mounted in a test fixture, which consisted of an alumina tube and an alumina ring. The cell was secured between the alumina tube and the alumina ring and spring-loaded to ensure good sealing between the cell and the alumina tube using a flexible gasket. A silver mesh and a Ni mesh, used as current collectors at the cathode and the anode, respectively, were spring-loaded against, respectively, the cathode and the anode. Measurements were carried out at 800°C, at 1 atm total pressure (both fuel and air), and at predetermined, constant total flow rates of fuel or fuel mixture and of air. The cell was reduced *in situ* at 800°C in a 10% H₂ + 90% N₂ mixture for several hours prior to measurements. The fuel flow rate was maintained at 140 mL/min and the air flow rate was maintained at 550 mL/min in all experiments. Open-circuit potentials (OCPs) were measured under constant fuel flow over the anode and the airflow over the cathode.

Cell performance was measured using various fuel gas mixtures, which included as-received H₂ (straight from the as-received cylinders, 99.99% pure H₂), as-received CO (straight from the as-received cylinders, 99.99% pure CO), H₂ + CO mixtures, H₂ diluted with He, N₂, CO₂, H₂O, and CO diluted with CO₂. Current-voltage (I-V) curves were measured at various diluent concentrations, *i.e.*, at various partial pressures of the diluent, while the total flow rate of fuel mixture was kept constant. Current densities were calculated based on the cathode area. The fact that cathode area is different from the anode surface exposed to fuel introduces a small error (typically <10%) in the power density. This issue has been addressed in detail elsewhere.¹³ Cell tests with as-received hydrogen were conducted without bubbling through a water bubbler.

Cell characterization.—Porosity of the Ni-YSZ anode was measured using the Archimedes method. The tested cell was broken into several small pieces. Dry weight, W_{dry} , wet weight, W_{wet} , and weight in water, W_{water} , were measured using a high-accuracy balance. Wet weight was measured (in air) soon after the surface of the sample was wiped dry, after boiling in water for 2 h. Porosity was calculated according to the equation

$$\text{Porosity} = \frac{W_{wet} - W_{dry}}{W_{wet} - W_{water}} \quad [1]$$

One of the fractured pieces was evacuated (to remove air from the pores) and impregnated with an epoxy. After hardening the epoxy, the sample was polished down to 1 μm finish. The microstructure of the cell was examined using scanning electron microscopy (SEM) and the mean pore radius was determined by quantitative stereology.¹⁴

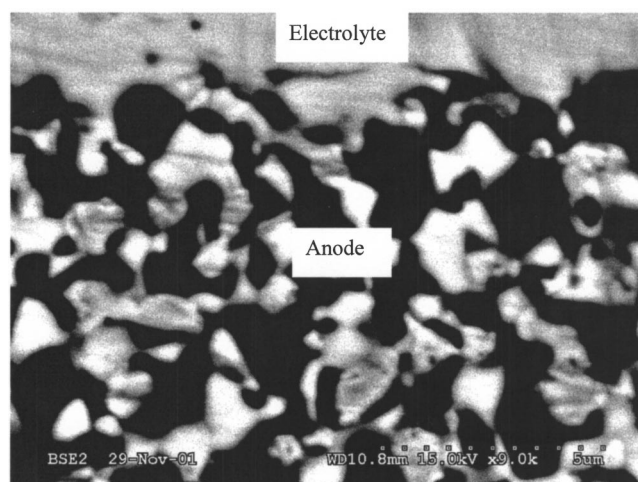


Figure 1. An SEM micrograph of a polished section of the Ni+YSZ anode (after impregnating with an epoxy).

Results

An SEM micrograph of a polished section of the Ni-YSZ anode is shown in Fig. 1. Figures 2-4 show cell voltage *vs.* current density, and power density *vs.* current density traces with as-received H₂, and H₂ diluted with various concentrations of He, N₂, and CO₂. For as-received H₂ as the fuel, the OCP was around 1.05 V, the maximum power density was about 1.7 W/cm², and there was no obvious limiting current density, even at the highest current density of 4.5 A/cm² at which measurements were made. When H₂ was diluted with various diluents, the general trend was similar for each diluent, namely: (i) with increasing dilution the open-circuit voltage (OCV) decreased, and (ii) the maximum power density as well as the maximum current density decreased. At high diluent concentrations, substantial concentration polarization was present as evidenced by the observation of a limiting current density. Since the cathode conditions were kept the same, the observed changes in performance with different diluents and their concentrations could be solely attributed to changes made in anodic conditions.

A comparison of Fig. 2 (H₂-He), 3 (H₂-N₂), 4 (H₂-CO₂), and 5 (H₂-H₂O) shows that the maximum power density achieved at the highest concentration of the diluent (~78-81%) was the highest for H₂-He mixtures (~0.75 W/cm²) and the lowest for H₂-CO₂ mixtures (~0.3 W/cm²). Also, the corresponding short-circuit current

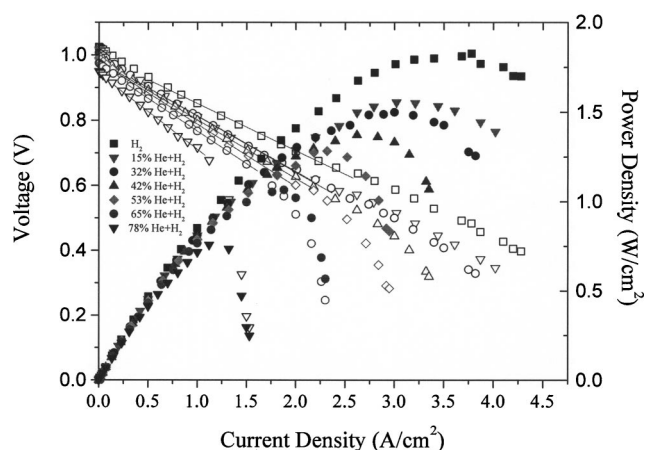


Figure 2. Voltage and power density *vs.* current density at 800°C with as-received H₂ and H₂ diluted with He as fuel.

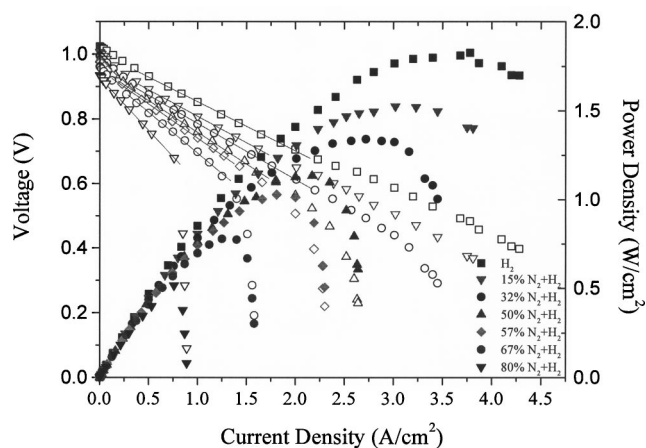
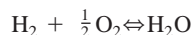


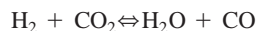
Figure 3. Voltage and power density vs. current density at 800°C with as-received H₂ and H₂ diluted with N₂ as fuel.

density was the highest for H₂-He mixture (~1.55 A/cm²) and the lowest for H₂-CO₂ mixture (~0.7 A/cm²). The highest power density measured was ~1.7 W/cm² for this cell with as-received H₂ as the fuel. A comparison of H₂-He and H₂-N₂ mixtures, wherein the diluent is inert, shows that the maximum power density at the highest diluent concentration is ~0.75 W/cm² for H₂-He and ~0.5 W/cm² for H₂-N₂ mixtures. Also, the corresponding anode-limiting current densities were ~1.55 A/cm² for H₂-He mixture and ~0.85 A/cm² for H₂-N₂ mixture of similar diluent concentrations.

As seen in Fig. 4 and 5, the OCV exhibited a stronger dependence on the diluent concentration when the diluent was either CO₂ or H₂O, consistent with expectations as the diluents in these cases are not inert, and enter into chemical reactions of the following type
In H₂-H₂O mixtures



and in H₂-CO₂ mixtures



until the respective reaction equilibria are established.

Figure 6 shows cell performance curves for gas mixtures containing CO and CO₂ as the fuel. The maximum power density measured with as-received CO as the fuel was ~0.7 W/cm², which is

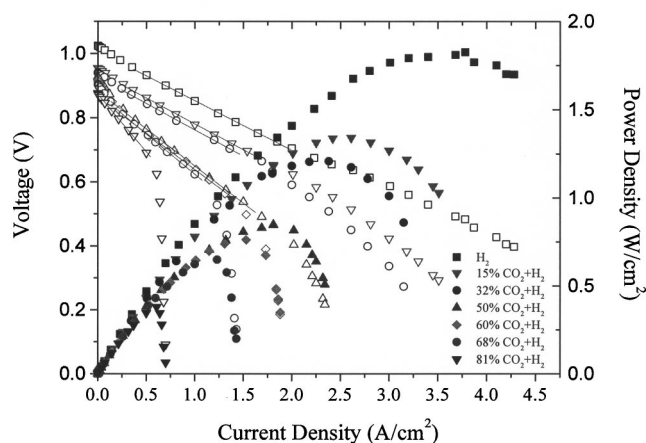


Figure 4. Voltage and power density vs. current density at 800°C with as-received H₂ and H₂ diluted with CO₂ as fuel.

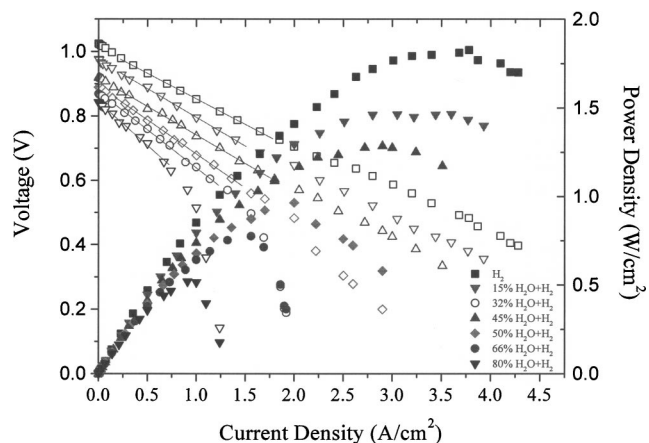


Figure 5. Voltage and power density vs. current density at 800°C for H₂-H₂O binary system with various concentrations of H₂O.

considerably lower than that with as-received H₂ as the fuel (Fig. 2-5). For the gas mixture containing 18% CO+82% CO₂, the maximum power density was only ~0.1 W/cm², and the corresponding limiting current density was only ~0.2 A/cm². An examination of Fig. 2-6 shows that a limiting current behavior is observed in all cases at higher diluent concentrations. The limiting current density, i_{as} , for each case is plotted vs. the partial pressure of the fuel gas (either H₂ or CO) in Fig. 7. It is seen that the dependence of i_{as} on the respective partial pressure (p_{H_2} or p_{CO}) is close to linear, with H₂-He fuel (or H₂-H₂O-He mixtures) exhibiting the highest i_{as} and the highest slope, and the CO-CO₂ mixtures exhibiting the lowest i_{as} and the lowest slope.

Figure 8 shows the performance curves with H₂ + CO gas mixtures as the fuel, where the composition was varied between ~100% (as-received) H₂ and ~100% (as-received) CO. The OCV is essentially independent of the relative proportions of H₂ and CO. The maximum power density varied between ~1.7 W/cm² for 100% H₂ to ~0.7 W/cm² for 100% CO. Note that the maximum power density for CO concentrations less than ~55% ranges between ~1.5 and ~1.7 W/cm²; and for CO concentrations between 68 and 100%, the maximum power density ranges between ~1.2 and ~0.7 W/cm².

Discussion

Thermodynamic calculation of OCVs.—The thermodynamic OCV of a fuel cell, which is the Nernst potential, is given by

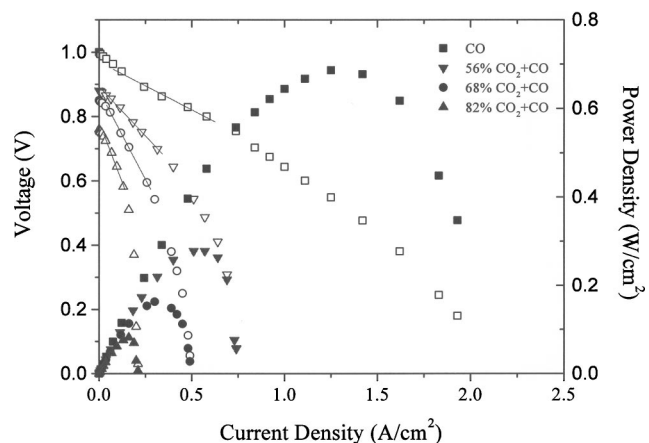


Figure 6. Voltage and power density vs. current density at 800°C for CO-CO₂ binary system with various concentrations of CO₂.

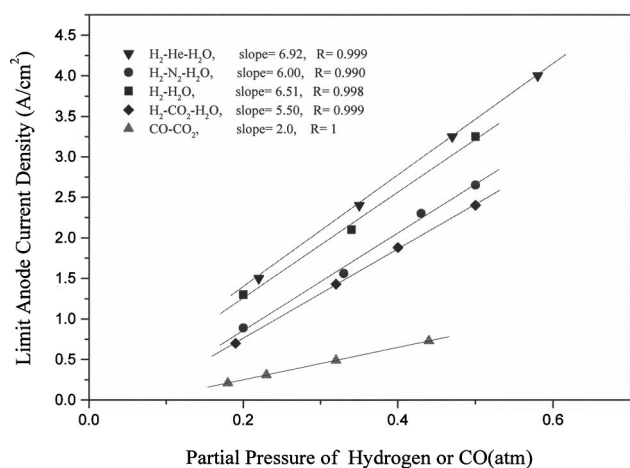


Figure 7. Anode limiting current density vs. partial pressure of H₂ or CO at 800°C.

$$E = \frac{RT}{4F} \ln \left(\frac{p_{\text{O}_2(\text{cathode})}}{p_{\text{O}_2(\text{anode})}} \right) \quad [2]$$

where $p_{\text{O}_2(\text{cathode})}$ is the partial pressure of oxygen at the cathode (under open-circuit conditions), which is 0.21 atm when air is used as the oxidant; $p_{\text{O}_2(\text{anode})}$ is the partial pressure of oxygen in fuel at the anode (under open-circuit conditions). For example, when H₂ is the fuel



at equilibrium, the partial pressure of oxygen at the anode, $p_{\text{O}_2(\text{anode})}$ is given as

$$\ln p_{\text{O}_2(\text{anode})} = \frac{2\Delta G_3^0}{RT} + 2 \ln \left(\frac{p_{\text{H}_2\text{O}}}{p_{\text{H}_2}} \right) \quad [4]$$

where ΔG_3^0 is the standard free energy of Reaction 3. The ΔG_3^0 is -188.165 kJ/mol at 800°C.¹⁵ At various partial pressures of H₂ and H₂O, $p_{\text{O}_2(\text{anode})}$ can be calculated from Eq. 4 and the OCV can be determined using Eq. 2.

Figure 9 shows the calculated $p_{\text{O}_2(\text{anode})}$ (except for as-received

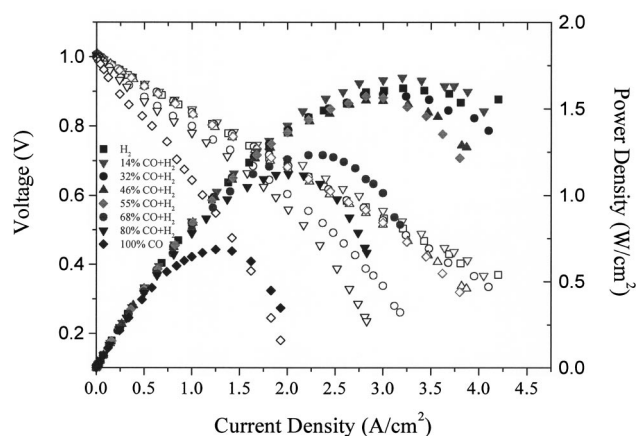


Figure 8. Voltage and power density vs. current density at 800°C for H₂-CO mixtures as fuel with various concentrations of CO.

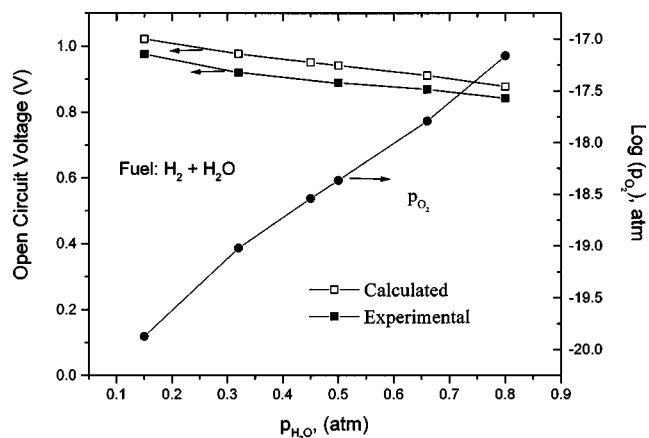


Figure 9. Partial pressure of oxygen at the anode and OCV as a function of $p_{\text{H}_2\text{O}}$ for H₂-H₂O at 800°C.

H₂, whose water content was not known), the calculated OCV, and the experimentally measured OCV as a function of $p_{\text{H}_2\text{O}}$. The partial pressure of oxygen at the anode increases from 10^{-20} atm to 10^{-17} atm, and the calculated OCV decreases from 1.021 to 0.877 V, when the $p_{\text{H}_2\text{O}}$ increases from 0.15 to 0.8 atm. The measured OCV, in general, exhibits the same trend as the calculated one, although it is about 50 mV lower than the calculated OCV. For the reaction



the standard free energy, ΔG_5^0 , is -189.65 kJ/mol.¹⁵ At p_{CO} lower than 0.8 atm, the disproportionation reaction



for which the standard free energy change is $\Delta G_6^0 = 17.63$ kJ/mol,¹⁵ should not occur at 800°C and 1 atm pressure, based on a thermodynamic calculation. For values of p_{CO} less than 0.8 atm, the partial pressures of CO and CO₂ in the initial gas mixture were used to estimate the equilibrium partial pressure of oxygen at the anode, namely, $p_{\text{O}_2(\text{anode})}$, using the following equation

$$\ln p_{\text{O}_2(\text{anode})} = \frac{2\Delta G_5^0}{RT} + 2 \ln \left(\frac{p_{\text{CO}_2}}{p_{\text{CO}}} \right) \quad [7]$$

For values of p_{CO} greater than 0.8 atm, first the partial pressures of CO and CO₂ according to the disproportionation reaction, Reaction 6, were estimated. Then $p_{\text{O}_2(\text{anode})}$ was estimated using the corresponding values of the partial pressures of CO and CO₂ and Eq. 7. Finally, the OCV was calculated as a function of the partial pressure of CO₂ in the initial mixture, $p_{\text{CO}_2}^0$. The calculated $p_{\text{O}_2(\text{anode})}$, the calculated OCV, and the measured OCV are plotted as a function of $p_{\text{CO}_2}^0$ in Fig. 10. The trends in the measured OCV and the calculated OCV are similar, although the measured OCV is between 50 and 75 mV lower than the theoretical values.

For calculating $p_{\text{O}_2(\text{anode})}$ and OCV for H₂ + CO₂ gas mixtures as the fuel, the reverse gas shift reaction, namely



for which the standard free energy is $\Delta G_8^0 = 0.385$ kJ/mol at 800°C was considered. The corresponding equilibrium p_{CO} , p_{CO_2} , p_{H_2} , and $p_{\text{H}_2\text{O}}$ were calculated. Then the corresponding $p_{\text{O}_2(\text{anode})}$ was calculated using either the H₂-H₂O equilibrium or the CO-CO₂ equilibrium. Using the calculated $p_{\text{O}_2(\text{anode})}$, the OCV was estimated by

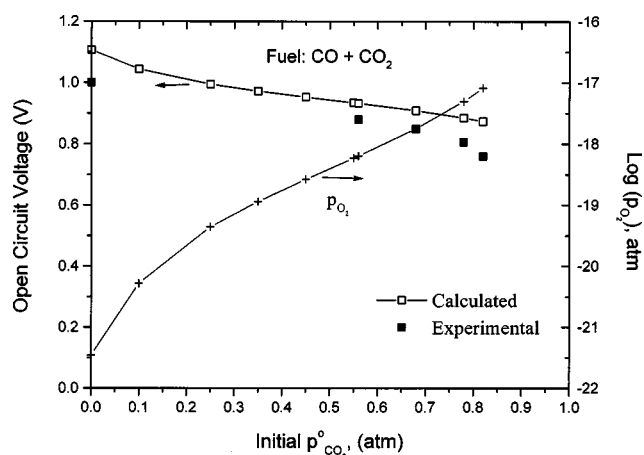


Figure 10. Partial pressure of oxygen at the anode and OCV as a function of p_{CO_2} for CO-CO₂ at 800°C.

Eq. 2. The calculated $p_{\text{O}_2(\text{anode})}$, the calculated OCV, and the measured OCV are plotted as a function of the partial pressure of CO₂ in the initial gas mixture, $p_{\text{CO}_2}^0$, in Fig. 11. As seen in the figure, the calculated and the measured OCV are in good agreement, especially for higher values of $p_{\text{CO}_2}^0$.

The thermodynamic calculations and comparison with experimental results show generally reasonable agreement between the calculated and experimental OCV values, insofar as the trends are concerned. However, the experimental values of the OCV are typically about 50 mV lower, and in some cases as much as 100 mV lower. There are a couple of possibilities for this discrepancy. (i) There may have been a few pinholes in the YSZ film. (ii) The sealing may not have been perfect. A lower OCV thus would imply a higher H₂O or CO₂ pressure and a correspondingly higher partial pressure of oxygen at the anode, $p_{\text{O}_2(\text{anode})}$. Leakage is also the possible reason that OCV in H₂-He and H₂-N₂ mixtures is dependent upon the relative proportions of H₂ and inert gas. If there had been no leakage, ideally, it would be expected that the OCV would be essentially independent of the concentration of inert diluent, He or N₂. In principle, using the measured OCV, this $p_{\text{O}_2(\text{anode})}$ can be calculated and thus the relative amount of water (or CO₂) present in the fuel can be estimated. However, as the general trend in measured OCV is consistent with calculations (and expectations) and signifi-

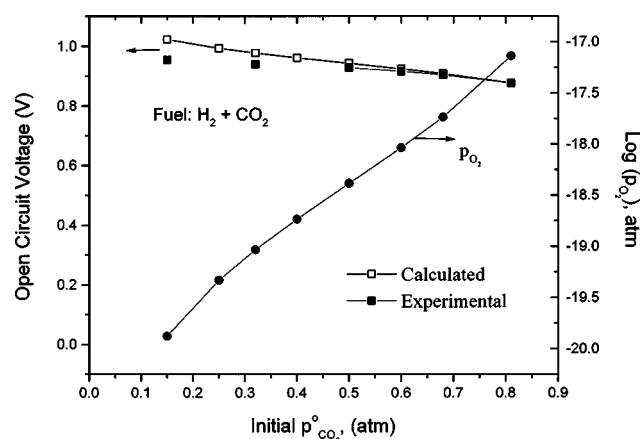


Figure 11. Partial pressure of oxygen at the anode and OCV as a function of p_{H_2} for H₂-CO₂ at 800°C.

cant uncertainties may exist in such calculations, no corrections for leakage were made, and the data reported are as measured.

Gas transport in porous anodes.—Gas transport through porous electrodes and correlation with electrochemical performance for binary gases, H₂-H₂O in the anode and O₂-N₂ in the cathode, have been addressed in detail.² There are two main fluxes contributing to mass transport in a porous electrode: a diffusive and a viscous flux. In general, the viscous flow, which is driven by a pressure gradient, is negligible compared to the diffusive flow in porous electrodes. Therefore, gas transport in porous electrodes is mainly due to diffusion, which includes free molecular or Knudsen flow, and a continuum flow.

The general diffusion process for a multicomponent gas system is described by the Stefan-Maxwell equation

$$\frac{N_i}{D_{K,i}} + \sum_{\substack{j=1 \\ j \neq i}} \frac{X_j N_i - X_i N_j}{D_{ij}} = -\frac{P}{RT} \frac{dX_i}{dx} \quad [9]$$

where N_i and N_j are molar fluxes of components i and j (no. mol/cm² s), respectively, $D_{K,i}$ and D_{ij} are the Knudsen diffusion coefficient for component i and the binary diffusion coefficient for components i and j , respectively, X_i and X_j are the mole fractions of components i and j , respectively, P is the total pressure, R is the gas constant, T is the absolute temperature, and x is the coordinate along the diffusion direction. Knudsen diffusion is due to molecule-to-wall collision, which predominates over molecule-to-molecule collision when the pore size is smaller than the mean free path.¹⁰ The Knudsen diffusion coefficient can be computed according to the kinetic theory of gases, using the following formula

$$D_{K,i} = \frac{2}{3} \left(\frac{8RT}{\pi M_i} \right)^{1/2} \bar{r} \quad [10]$$

where \bar{r} is the mean pore radius and M_i is the molecular weight of the diffusing gas. The binary diffusion coefficient, D_{ij} , is generally experimentally measured or calculated using the Chapman-Enskog equation,¹⁶ if it is not available experimentally. According to the Chapman-Enskog model, the binary diffusion coefficient in cm²/s is given by¹⁶

$$D_{ij} = \frac{1.86 \times 10^{-3} T^{3/2} \left(\frac{1}{M_i} + \frac{1}{M_j} \right)^{1/2}}{P \Omega \sigma_{ij}^2} \quad [11]$$

where Ω is the collision integral (dimensionless), σ_{ij} is the average collision diameter (in angstroms), M_i and M_j are molecular weights of component i and j , respectively, and P is the total pressure (in atm). Using Ω and σ_{ij} data from Cussler,¹⁶ the calculated D_{ij} for various gaseous species and at several temperatures are listed in Table I, along with some experimental values from the literature for comparison.^{15,17,18} Slight difference, usually less than 10%, is often observed between the calculated values and the experimental values over a range of temperatures between room temperature and 473 K. Little data are available at higher temperatures. Hence, D_{ij} at 800°C were estimated using the Chapman-Enskog model.

In the present experiments, the mean pore radius of the Ni-YSZ electrode was estimated from SEM micrographs (Fig. 1) to be ~ 0.5 μm . The calculated Knudsen diffusion coefficients at 800°C for H₂ and CO through the Ni-YSZ porous electrode are 11.3 and 3 cm²/s, respectively. These values are comparable to the respective binary diffusion coefficient of H₂-He, which is 13.3 cm²/s, and CO-CO₂, which is 1.41 cm²/s at the same temperature (Table I). This indicates that Knudsen diffusion is an important process in the present porous anodes with 0.5 μm mean pore radius and should be taken into account.

For a ternary system such as H₂-He-H₂O, the H₂ molar flux from Eq. 9 is given by

Table I. Calculated binary diffusion coefficients from the Chapman-Enskog equation and comparison with some experimental data from the literature.

D_{ij} (cm ² /s)	H ₂ -He	H ₂ -N ₂	H ₂ -CO ₂	H ₂ -H ₂ O	H ₂ -CO	CO-CO ₂
293K	1.535	0.722	0.604	0.738	0.726	0.149
	1.53 ^a	0.728 ^a	0.651 ^b	0.834 ^b	0.735 ^a	0.162 ^c
	1.49 ^c	0.772 ^c			0.772 ^c	
473K	3.417	1.626	1.395	1.819	1.642	0.349
	3.45 ^a	1.631 ^a	1.513 ^b	1.996 ^b	1.651 ^a	0.384 ^c
	3.39 ^c	1.743 ^c	1.473 ^c		1.743 ^c	
1073K	13.29	6.303	5.56	7.704	6.373	1.408

^a From Ref. 17.^b From Ref. 18.^c From Ref. 15.

$$\frac{N_{H_2}}{D_{K,H_2}} + \frac{X_{He}N_{H_2} - X_{H_2}N_{He}}{D_{H_2,He}} + \frac{X_{H_2O}N_{H_2} - X_{H_2}N_{H_2O}}{D_{H_2,H_2O}} = -\frac{P}{RT} \frac{dX_{H_2}}{dx} \quad [12]$$

Under steady-state conditions, $N_{H_2O} = -N_{H_2}$ and $N_{He} = 0$. Thus

$$N_{H_2} \left(\frac{1}{D_{K,H_2}} + \frac{X_{He}}{D_{H_2,He}} + \frac{1 - X_{He}}{D_{H_2,H_2O}} \right) = -\frac{P}{RT} \frac{dX_{H_2}}{dx} \quad [13]$$

From Eq. 13, H₂ flux can be written in a similar form as Fick's equation by

$$N_{H_2} = -\frac{PD_{H_2}}{RT} \frac{dX_{H_2}}{dx} \quad [14]$$

where D_{H_2} is defined as the H₂ diffusion coefficient in the H₂-H₂O-He ternary system, and is given by

$$D_{H_2} = \left(\frac{1}{D_{K,H_2}} + \frac{X_{He}}{D_{H_2,He}} + \frac{1 - X_{He}}{D_{H_2,H_2O}} \right)^{-1} \quad [15]$$

When $X_{He} = 0$, *i.e.*, for H₂-H₂O binary system, the H₂ diffusion coefficient becomes

$$D_{H_2} = \left(\frac{1}{D_{K,H_2}} + \frac{1}{D_{H_2,H_2O}} \right)^{-1} \quad [16]$$

Similarly, for the CO-CO₂ binary system, the CO diffusion coefficient is given by

$$D_{CO} = \left(\frac{1}{D_{K,CO}} + \frac{1}{D_{CO,CO_2}} \right)^{-1} \quad [17]$$

where $D_{K,CO}$ and D_{CO,CO_2} are the Knudsen diffusion coefficient of CO and the binary diffusion coefficient of CO-CO₂, respectively.

The preceding equations for diffusion coefficients are for transport in a multicomponent gas system and do not account for the volume fraction of porosity and the tortuous nature of path through porous bodies. When the transport occurs through a porous body, the interaction of gaseous species with the porous matrix must be included. The simplest approach for taking this into account is to modify the diffusion coefficients by the volume fraction porosity, V_v , and the tortuous nature of the actual transport, characterized by the so-called tortuosity factor, τ .¹⁶ The resulting diffusion coefficients or diffusivities are termed effective diffusion coefficients or effective diffusivities. For H₂ and CO, the corresponding effective diffusivities are given by¹⁶

$$D_{H_2,eff} = \frac{V_v}{\tau} D_{H_2} \quad [18]$$

and

$$D_{CO,eff} = \frac{V_v}{\tau} D_{CO} \quad [19]$$

where D_{H_2} and D_{CO} are given, respectively, by Eq. 15 or 16 and 17.

As shown on the right side of Eq. 15, for a ternary system D_{H_2} is not only a function of diffusion coefficients, D_{K,H_2} , $D_{H_2,He}$, and D_{H_2,H_2O} , but is also a function of the mole fraction of the diluent gas, X_{He} . If X_{He} varies from position to position along the diffusion direction, D_{H_2} will be a function of position. The variation of X_{He} as a function of the position, x , can be determined by solving Eq. 9 for the He flux, N_{He} , given by

$$\frac{N_{He}}{D_{K,He}} + \frac{X_{H_2}N_{He} - X_{He}N_{H_2}}{D_{He,H_2}} + \frac{X_{H_2O}N_{He} - X_{He}N_{H_2O}}{D_{He,H_2O}} = -\frac{P}{RT} \frac{dX_{He}}{dx} \quad [20]$$

Because the net flow of He, N_{He} , is zero and $N_{H_2} = -N_{H_2O}$ in steady state, Eq. 20 becomes

$$N_{H_2} \left(\frac{1}{D_{He,H_2O}} - \frac{1}{D_{He,H_2}} \right) X_{He} = -\frac{P}{RT} \frac{dX_{He}}{dx} \quad [21]$$

Integration of Eq. 21 gives

$$X_{He}^{l_a} = X_{He}^o \exp \left[\frac{RTN_{H_2}l_a}{P} \left(\frac{1}{D_{He,H_2}} - \frac{1}{D_{He,H_2O}} \right) \right] \quad [22]$$

where l_a is the anode thickness, X_{He}^o is the mole fraction of He at $x = 0$, and $X_{He}^{l_a}$ is the mole fraction of He at $x = l_a$. The case of interest is that of a porous anode. Thus, the diffusivities must be those corrected for porosity and tortuosity factor. Thus, the applicable equation is actually

$$X_{He}^{l_a} = X_{He}^o \exp \left[\frac{RTN_{H_2}l_a}{P} \left(\frac{1}{D_{He,H_2,eff}} - \frac{1}{D_{He,H_2O,eff}} \right) \right] \quad [23]$$

Equation 22 and 23 show that X_{He} varies exponentially as a function of position. For the case of transport through space, in the absence of a porous body, the calculated variation of X_{He} along the electrode is very small. Using the estimated diffusion coefficients from the Chapman-Enskog model, $D_{He,H_2} = 13.29$ cm²/s and $D_{He,H_2O} = 4.07$ cm²/s, the X_{He} at the electrode/electrolyte interface ($l_a = 0.1$ cm) is about 0.8% lower than the bulk molar value of He, X_{He}^o , at a current density of 1 A/cm², *i.e.*, for a molar flux of 5.18×10^{-6} mol/cm²s. Even at a current density close to the anode limiting current density, 3 A/cm², X_{He} is only 3% lower than X_{He}^o . Such, however, is not the case for a porous body. For transport through porous anodes, Eq. 23 must be used. The corresponding variation in X_{He} is $\sim 10\%$ at a current density of 1 A/cm² and $\sim 20\%$ at a current density of 3 A/cm². Though this variation is not insignificant, for simplicity we neglect this aspect and assume that the diffusion coefficient of H₂ is independent of position.

If the electrode microstructure is not a function of position, *i.e.*, V_v and τ are constant, integration of Eq. 14, using effective diffusivities, gives a simple equation for H_2 flux in a ternary system, similar to that for a binary system, namely

$$N_{H_2} = -\frac{PD_{H_2,eff}}{RTl_a}(X_{H_2} - X'_{H_2}) \quad [24]$$

where X'_{H_2} and X_{H_2} are the mole fractions of H_2 over the anode surface ($x = 0$) and at the anode/electrolyte interface ($x = l_a$), and $D_{H_2,eff}$ is the effective ternary diffusion coefficient as defined by Eq. 15 and 18. Replacing mole fractions with partial pressures, Eq. 24 becomes

$$N_{H_2} = -\frac{D_{H_2,eff}}{RTl_a}(p_{H_2} - p'_{H_2}) \quad [25]$$

where p'_{H_2} and p_{H_2} are the partial pressure of H_2 over the anode surface ($x = 0$) and the partial pressure of H_2 at the anode/electrolyte interface ($x = l_a$), respectively. Assuming gases are well mixed above the anode, similar to the situation in a continuously stirred tank reactor (CSTR), p'_{H_2} is given by

$$p'_{H_2} = p_{H_2}^0 - \frac{N_{H_2}A}{m_T}P \quad [26]$$

where $p_{H_2}^0$ is the initial (incoming fuel) partial pressure of H_2 , A is the electrode area (1.1 cm^2), m_T the total molar flow rate of fuel and diluent, and P is total pressure. Substituting for p'_{H_2} from Eq. 26 into Eq. 25 gives

$$N_{H_2} = -\frac{D_{H_2,eff}}{RTl_a}\left(p_{H_2} - p_{H_2}^0 + \frac{N_{H_2}A}{m_T}P\right) \quad [27]$$

Rearranging Eq. 27, H_2 molar flux is given by

$$N_{H_2} = -\frac{\frac{D_{H_2,eff}(p_{H_2} - p_{H_2}^0)}{RTl_a}}{1 + \frac{D_{H_2,eff}AP}{RTl_a m_T}} \quad [28]$$

A maximum in H_2 flux occurs when p_{H_2} at the interface approaches zero. This maximum flux is given by

$$N_{H_2,max} = \frac{\frac{D_{H_2,eff}p_{H_2}^0}{RTl_a}}{1 + \frac{D_{H_2,eff}AP}{RTl_a m_T}} \quad [29]$$

The net current density passing through the cell is related to the net hydrogen flux arriving at the anode/electrolyte interface, and is given by

$$i = 2FN_{H_2} = -\frac{2FD_{H_2,eff}(p_{H_2} - p_{H_2}^0)}{RTl_a} \frac{1}{1 + \frac{D_{H_2,eff}AP}{RTl_a m_T}} \quad [30]$$

For the maximum possible hydrogen flux given by Eq. 29, there will be a corresponding maximum in current density, which is the anode limiting current density given by

$$i_{as} = \frac{\frac{2FD_{H_2,eff}p_{H_2}^0}{RTl_a}}{1 + \frac{D_{H_2,eff}AP}{RTl_a m_T}} \quad [31]$$

In all experiments, when the mole percent of the diluent was more than 40%, a limiting current density was observed. From the experimentally measured anode limiting current density, one can estimate the effective diffusion coefficients for H_2 for several diluents and at various concentrations by rearranging Eq. 31 as follows

$$D_{H_2,eff} = \frac{i_{as}}{\frac{2Fp_{H_2}^0}{RTl_a} - \frac{i_{as}AP}{RTl_a m_T}} \quad [32]$$

Also, for CO-CO₂ mixtures, Eq. 32 can be used with $p_{H_2}^0$ replaced by p_{CO}^0 , and $D_{H_2,eff}$ replaced by $D_{CO,eff}$. Table II lists the calculated diffusion coefficients from Equation 15-17, the estimated effective H_2 (and CO) diffusion coefficients from Eq. 32, and the experimentally measured i_{as} values from the voltage-current density polarization curves.

From Table II, it is seen that the H_2 diffusion coefficient, D_{H_2} , for H_2 - H_2O is about five times larger than that for CO-CO₂, D_{CO} . For H_2 - H_2O , the effective diffusion coefficient estimated using Eq. 32, ranges from 0.470 to 0.506 cm²/s, almost independent of gas composition, consistent with Eq. 16. For CO-CO₂ mixtures, it varies from 0.063 to 0.090 cm²/s over the range of p_{CO} investigated. This suggests that mass transport of H_2 in H_2 - H_2O mixtures should be about five to six times faster than that of CO in CO-CO₂ mixtures. If CO is used as a fuel, the cell performance is expected to be lower than with H_2 as a fuel due to slow diffusion rate, regardless of other effects, such as the intrinsically low electrochemical activity of CO.

Prior work has shown that anodic concentration polarization for H_2 - H_2O gas mixtures is given by²

$$\eta_{conc} = -\frac{RT}{2F} \ln\left(1 - \frac{i}{i_{as}}\right) + \frac{RT}{2F} \ln\left(1 + \frac{p_{H_2}^0 i}{p_{H_2O}^0 i_{as}}\right) \quad [33]$$

It is readily seen that the corresponding equation for CO-CO₂ gas mixtures as a fuel is given by

$$\eta_{conc} = -\frac{RT}{2F} \ln\left(1 - \frac{i}{i_{as}}\right) + \frac{RT}{2F} \ln\left(1 + \frac{p_{CO}^0 i}{p_{CO_2}^0 i_{as}}\right) \quad [34]$$

Using Eq. 33 and 34,^a η_{conc} was calculated as a function of current density for a H_2 - H_2O mixture of composition 34% H_2 - 66% H_2O , and for a CO-CO₂ mixture of composition 32% CO - 68% CO₂, for which the corresponding anode limiting current densities were ~ 2 and $\sim 0.5 \text{ A/cm}^2$, respectively. The calculated concentration polarization is compared with the measured total polarization (by subtracting the ohmic contribution) in Fig. 12. It is readily seen that anodic concentration polarization is much greater in CO-CO₂ mixtures as compared to H_2 - H_2O mixtures. The difference between the measured total (excluding the ohmic) and the calculated anodic concentration polarization is attributed to anodic and cathodic acti-

^a Since the partial pressure of H_2 or CO at the anode/fuel interface is a function of the current density (using Eq. 26), one must strictly use p_{H_2} instead of $p_{H_2}^0$ (or p_{CO} instead of p_{CO}^0) in estimating the concentration polarization and attribute the remainder of the terms to polarization associated with the depletion of fuel. Here, the two terms are combined into a single equation describing concentration polarization, namely, Eq. 33 for H_2 as a fuel (or Eq. 34 for CO as a fuel).

Table II. Partial pressure of dilute gas, anode limiting current density, H₂ and CO diffusion coefficient, porosity, and tortuosity.

H ₂ -H ₂ O Binary System					
p_{H_2}	i_{as} (A/cm ²)	D_{H_2} (cm ² /s) (cal.)	$D_{H_2,eff}$ (cm ² /s) (exp.)	Porosity (%) (exp.)	Tortuosity
0.2	1.3	4.58	0.506	54	4.89
0.34	2.1	4.58	0.470	54	5.26
0.5	3.25	4.58	0.506	54	4.89
CO-CO ₂ Binary System					
p_{CO}	i_{as} (A/cm ²)	D_{CO} (cm ² /s) (cal.)	$D_{CO,eff}$ (cm ² /s) (exp.)	Porosity (%) (exp.)	Tortuosity
0.18	0.21	0.958	0.063	54	8.27
0.23	0.31	0.958	0.073	54	7.08
0.32	0.49	0.958	0.084	54	6.17
0.44	0.73	0.958	0.091	54	5.65
H ₂ -He-H ₂ O Ternary System					
p_{He}	i_{as} (A/cm ²)	D_{H_2} (cm ² /s) (cal.)	$D_{H_2,eff}$ (cm ² /s) (exp.)	Porosity (%) (exp.)	Tortuosity
0.78	1.5	5.677	0.545	54	5.62
0.65	2.4	5.458	0.550	54	5.35
0.53	3.25	5.269	0.558	54	5.10
0.42	4	5.108	0.556	54	4.96
H ₂ -N ₂ -H ₂ O Ternary System					
p_{N_2}	i_{as} (A/cm ²)	D_{H_2} (cm ² /s) (cal.)	$D_{H_2,eff}$ (cm ² /s) (exp.)	Porosity (%) (exp.)	Tortuosity
0.8	0.89	4.135	0.295	54	7.56
0.67	1.56	4.2	0.320	54	7.09
0.57	2.3	4.252	0.379	54	6.05
0.5	2.65	4.289	0.375	54	6.18
H ₂ -CO ₂ -H ₂ O Ternary System					
p_{CO_2}	i_{as} (A/cm ²)	D_{H_2} (cm ² /s) (cal.)	$D_{H_2,eff}$ (cm ² /s) (exp.)	Porosity (%) (exp.)	Tortuosity
0.81	0.7	3.858	0.230	54	9.00
0.68	1.43	3.957	0.296	54	7.20
0.6	1.88	4.021	0.317	54	6.84
0.5	2.4	4.103	0.327	54	6.77

vation polarizations and cathodic concentration polarization. The cathodic polarization (activation+concentration) is the same for the two curves. For the test with H₂-H₂O as the fuel, at 0.25 A/cm² the difference between the measured and the calculated polarization

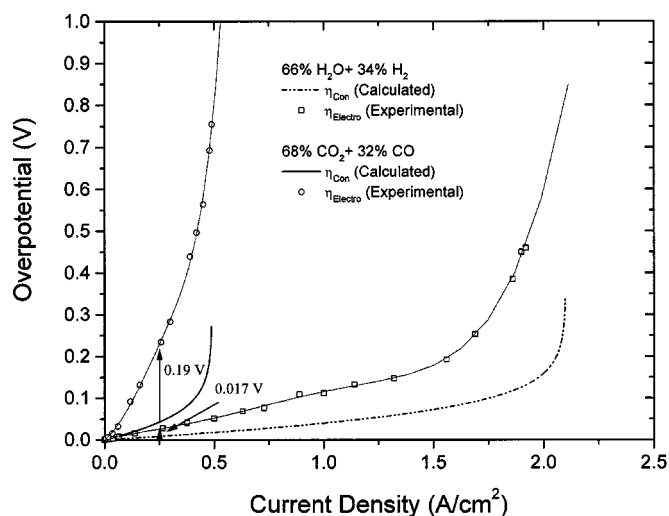


Figure 12. Comparison of the measured total polarization (less the ohmic contribution) as a function of current density vs. calculated concentration polarization for: (a) ~34% H₂ + ~66% H₂O and (b) ~32% CO + ~68% CO₂.

(Eq. 33) is ~0.017 V, which includes: (a) cathodic concentration polarization, (b) cathodic activation polarization, and (c) anodic activation polarization. At the same current density, the difference between the measured and calculated polarization (Eq. 34) is ~0.19 V for CO-CO₂ as the fuel. However, the cathodic polarizations for (a) and (b) are identical for the two tests. Clearly, greater polarization with the CO-CO₂ mixture, beyond what can be attributed to anodic concentration polarization, is attributed to anodic activation polarization. That is, anodic activation polarization with CO-CO₂ gaseous mixture of the chosen composition at 0.25 A/cm² is ~0.173 V higher than that with H₂-H₂O gaseous mixture. This also suggests that Ni+YSZ is not a very good anode for CO as the fuel. Indeed, it has been reported in the literature that the electrochemical reaction rate of CO is slower than that of H₂ by at least a factor of two.¹² Comparison of performance curves for H₂-H₂O mixtures with CO-CO₂ mixtures from Fig. 5 and 6 shows that the lower performance with CO-CO₂ mixtures cannot be attributed entirely to concentration polarization. Thus, although CO does not poison SOFC anodes unlike PEM fuel cells, its low electrochemical activity, at least with nickel-based anodes, and high concentration polarization suggests that it is not an ideal fuel for SOFCs if a high power density is a requirement.

The estimated D_{H_2} using the Chapman-Enskog model and the analysis of multicomponent transport as a function of diluent type and concentration is given in Table II. The experimentally determined $D_{H_2,eff}$ from the anode-limiting current behavior via Eq. 32, which includes the effects of porosity and tortuosity, are also given in Table II. Note that for He as a diluent, the estimated D_{H_2} is higher

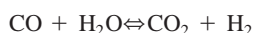
than with N₂ as the diluent. Table II also shows that estimated $D_{H_2,eff}$ is also similarly higher for He as a diluent compared to N₂ as a diluent. Similar trends are observed for CO₂ as a diluent. Finally, for CO-CO₂ mixtures, the estimated D_{CO} is much lower and so is the $D_{CO,eff}$. In the case of either N₂ or CO₂ as a diluent, it is also seen that the trends in D_{H_2} and $D_{H_2,eff}$ as a function of composition are similar. That is, the results indicate that except for He, H₂ diluted with either N₂ or CO₂ not only lowers the partial pressure of H₂ but also reduces the effective H₂ diffusion coefficient. Thus, the diluent can lower cell performance in two ways, reduced p_{H_2} and reduced transport kinetics. From the experimental results (Fig. 3), at 32% N₂ dilution the maximum power density was reduced by more than 30%. It was even worse for CO₂ dilution with almost 40% reduction of the maximum power density (Fig. 4) at the same diluent concentration. This suggests when either partial oxidation or auto-thermal reforming is used for processing fuel, nitrogen introduced into fuel leads to a lowering of diffusive transport, in addition to fuel dilution. The present work also shows that if in a reforming stage most of the CO is converted to CO₂ via a gas shift reaction, in addition to fuel dilution there is also an adverse effect on diffusive transport.

Using D_{H_2} , $D_{H_2,eff}$, D_{CO} , and $D_{CO,eff}$ and the measured porosity of 54% for the Ni-YSZ anode, the tortuosity factor of the anode, τ , was calculated from Eq. 18 and 19. All of the tortuosity factors fall between 5.0 and 7.0 from H₂-H₂O and CO-CO₂ binary system measurements (with the exception of one value which is over 8.0) and from H₂-H₂O with He, N₂ and CO₂ dilution (with the exception of one value which is 9). The observation that tortuosity factor is on the order of ~5 to ~7 justifies the use of effective diffusivities. At the same time, the observation that the estimated tortuosity factor does exhibit some variability suggests that it may include effects in addition to purely geometric factors (such as, possibly, adsorption and surface diffusion). A value of five measured by a different method for a Ni-YSZ anode has been reported in the literature.¹¹ This suggests that the possible effects of adsorption/desorption and surface diffusion must be small in anodes of the present study.

Cell performance with H₂ + CO mixture as the fuel.—The cell performance with as-received CO as fuel was poor because of slow diffusion and slow electrochemical reaction rate, as discussed earlier. However, the cell performance on H₂ + CO even when CO concentration was as high as 55% was very high, close to that with as-received H₂ (Fig. 8) and quite high with CO content as high as 80%. The diffusion coefficient of H₂ in H₂-H₂O-CO ternary mixtures (ignoring the effects of CO₂) may be given by

$$D_{H_2} = \left(\frac{1}{D_{K,H_2}} + \frac{X_{CO}}{D_{H_2,CO}} + \frac{1 - X_{CO}}{D_{H_2,H_2O}} \right)^{-1} \quad [35]$$

The calculated D_{H_2} ranges between 4.17 and 4.31 cm²/s for CO mole fraction between 0.8 and 0.5, which is similar to that for H₂-H₂O-N₂. However, the observed performance with H₂-CO is much superior to that with H₂-H₂O-N₂ mixtures as the fuel. This is consistent with expectations because a shift reaction is expected in H₂-CO gas mixtures during cell operation. At 800°C the standard Gibbs free energy for the gas shift reaction



is only -0.368 kJ/mol.¹⁵ However, the reaction rate constant is very high as reported in the literature and thus it may be assumed that the shift reaction at the anode/electrolyte interface is at equilibrium.¹¹ Thus, for a fuel gas composition containing greater than 50% H₂ (and balance CO), it can be argued that H₂O produced by the electrochemical oxidation of H₂ is more than sufficient to react with CO present to form H₂ and CO₂. In such a case, there should be little difference in performance when compared to pure H₂ as fuel (with

the exception of a small difference related to differences in concentration polarization). There is very little difference in performance with fuels ranging in composition from ~100% H₂ and ~45% H₂ + ~55% CO, as seen in Fig. 8. For compositions of fuel containing substantially greater than 50% CO, the H₂O produced by the electrochemical oxidation of H₂ is not sufficient to shift most of the CO to CO₂. The remaining CO has to be oxidized electrochemically to CO₂, for which polarization is observed to be much greater (Fig. 6). Indeed, Fig. 8 shows that the performance is much worse with fuels containing ~68% CO + ~32% H₂ and ~80% CO + ~20% H₂.

Conclusions

Based on the present work, the following conclusions are drawn:

1. Anode-supported SOFCs exhibit substantial effect of an inert gas diluent in the fuel on concentration polarization, consistent with expectations based on multicomponent gas diffusion in porous bodies. Specifically, anodic concentration polarization is lower with an inert gas diluent of low molecular weight (such as He) than an inert gas diluent of higher molecular weight (such as N₂).

2. For a sufficiently high concentration of the diluent, the voltage vs. current density traces exhibits anode limiting current density behavior, characterizing a rapid drop of voltage at a critical current density. This current density was used to estimate the corresponding effective diffusivities.

3. Electrochemical performance with CO + CO₂ gas mixtures is much worse than fuel gas mixtures containing H₂. This is rationalized in part on higher anodic concentration polarization and slower electrochemical oxidation of CO. The results show that Ni + YSZ is an excellent anode for H₂-containing fuel, but not for CO.

4. Studies on cell performance with CO + H₂ gas mixtures as fuel show that water gas shift reaction plays a major role. Effectively, as long as the H₂ content is greater than ~50%, high performance is maintained by producing additional H₂ through the shift reaction. As a result, the cell performance with essentially pure H₂ is about the same as that with a H₂ + CO gaseous mixture as fuel, as long as the CO concentration is not too high.

Acknowledgments

This work was supported by the U.S. Department of Energy (NETL) under contract no. DE-AC26-99FT40713.

The University of Utah assisted in meeting the publication costs of this article.

List of Symbols

A	cathode area, cm ²
D_i	diffusion coefficient of gaseous species i , cm ² /s
$D_{K,i}$	knudsen diffusion coefficient of gaseous species i , cm ² /s
$D_{i,eff}$	effective diffusion coefficient of gaseous species i , cm ² /s
D_{ij}	binary diffusion coefficient of gaseous species i and j , cm ² /s
$D_{ij,eff}$	binary effective diffusion coefficient of gaseous species i and j , cm ² /s
E	ernst voltage, V
F	faraday constant, C/mol
ΔG°	standard free energy change, kJ/mol
i	current density, A/cm ²
i_{as}	anode-limiting current density, A/cm ²
l_a	anode thickness, cm
M_i	molecular weight of gaseous species i , g
m_T	total molar flow rate of fuel, mol/s
N_i	molar flux of gaseous species i , mol/cm ² s
p_i	partial pressure of gaseous species i , atm
R	ideal gas constant, J/mol K
T	temperature, K
V_v	volume fraction porosity
W	mass, g
x	coordinate along the diffusion direction, cm
X_i	mole fraction of gaseous species i

Greek

η	polarization, V
σ_{ij}	average collision diameter of gaseous species i and j , Å
τ	tortuosity factor
Ω	collision integral

References

1. S. DeSouza, S. J. Visco, and L. C. DeJonghe, *Solid State Ionics*, **98**, 57 (1997).
2. J. W. Kim, A. V. Virkar, K.-Z. Fung, K. Metha, and S. C. Singhal, *J. Electrochem. Soc.*, **146**, 69 (1999).
3. T. Tsai and S. A. Barnett, *Solid State Ionics*, **98**, 191 (1997).
4. Y. Jiang and A. V. Virkar, in *Ionic and Mixed Conducting Ceramics (IV)*, T. A. Ramanarayan, Editor, PV 2001-28, p. 374, The Electrochemical Society Proceedings Series, Pennington, NJ (2001).
5. E. P. Murray, T. Tsai, and S. A. Barnett, *Nature (London)*, **400**, 649 (1999).
6. S. Park, R. Cracium, J. M. Vohs, and R. J. Gorte, *J. Electrochem. Soc.*, **146**, 3603 (1999).
7. Y. Jiang and A. V. Virkar, *J. Electrochem. Soc.*, **148**, A701 (2001).
8. R. Peters, E. Riensche, and P. Cremer, *J. Power Sources*, **86**, 432 (2000).
9. E. A. Mason and A. P. Malinauskas, *Gas Transport in Porous Media: The Dusty Gas Model*, Elsevier, Amsterdam (1983).
10. R. R. Remick and C. J. Geankoplis, *Chem. Eng. Sci.*, **29**, 1447 (1974).
11. W. Lehnert, J. Meusinger, and F. Thom, *J. Power Sources*, **87**, 57 (2000).
12. H. Yakabe, M. Hishinuma, M. Uratani, Y. Matsuzaki, and I. Yasuda, *J. Power Sources*, **86**, 423 (2000).
13. Y. Jiang, A. V. Virkar, and F. Zhao, *J. Electrochem. Soc.*, **148**, A1091 (2001).
14. E. E. Underwood, *Quantitative Stereology*, Addison-Wesley, Reading, MA (1969).
15. D. R. Lide and H. V. Kehiaian, *CRC Handbook of Thermophysical and Thermochemical Data*, CRC Press, Inc., Boca Raton, FL (1994).
16. E. L. Cussler, *Diffusion-Mass Transfer in Fluid Systems*, Cambridge University Press, Cambridge, MA (1984).
17. S. Weissman and E. A. Mason, *J. Phys. Chem.*, **37**, 1289 (1962).
18. N. B. Vargaftik, *Handbook of Physical Properties of Liquids and Gases*, 2nd ed., Hemisphere Publication Corporation, Bristol, PA (1976).